| | |
|---|---|
| Please fill in the name of the event you are preparing this manuscript for. | SPE/IADC Drilling Conference 2019 |
| Please fill in your 6-digit SPE manuscript number. | SPE-194146-MS |
| Please fill in your manuscript title. | On the sealability of metal-to-metal seals with application to premium casing connections |

Please fill in your author name(s) and company affiliation.


| Given Name | Surname | Company |
|---|---|---|
| Dennis | Ernens | Shell Global Solutions International BV, University of Twente |
| Francesc | Peréz-Ràfols | Luleå University of Technology |
| Dennis | Van Hoecke | OCAS NV |
| Roel F. H. | Roijmans | Shell Global Solutions International BV |
| Egbert J. | van Riet | Shell Global Solutions International BV |
| John | Vande Voorde | OCAS NV |
| Andreas | Almqvist | Luleå University of Technology |
| Matthijn Bas | de Rooij | University of Twente |
| Serge Mathieu | Roggeband | Shell Global Solutions International BV |
| Willem Maarten | Van Haaften | Shell Global Solutions International BV |
| Marc | Vanderschueren | OCAS NV |
| Phillipe | Thibaux | OCAS NV |
| Henry Rihard | Pasaribu | Shell Global Solutions International BV |




## Abstract


Metal-to-metal seals are used in connections of casing in oil and gas wells. This paper describes the mechanisms of sealing of metal-to-metal seals as investigated using an experimental set-up and a sealability model. Experiments were conducted for a variety of thread compounds and applied pin/box surface coatings. The results were used to validate a numerical model for sealability. The stochastic model couples a contact mechanics model with a flow model and takes the influence of all the surface topography features into account. Once validated, the model was used together with the experimental results to explain the sealing mechanisms of metal-to-metal seals.

The sealing configuration is a face seal with an R=80 mm round-off radius pressing against a flat. The face seal specimens were manufactured from P110 tubing. The used test set-up is designed for investigating only the metal-to-metal seal of the connection. The set-up can carry out rotary sliding under constant load to simulate surface evolution during make-up and subsequently perform a leakage test. The sealing limit is determined by applying 700 bar fluid pressure and then gradually reducing the normal force until leakage is observed. The data is subsequently used to validate a previously published model.

The results indicate a strong dependence of the type of thread compound used on the onset of leakage. The thread compound affects the amount of wear and thus changes the surface topography of the interacting surfaces. It is shown that the sealability model is capable to predict the onset of leakage within the experimental accuracy. The model shows further that certain surface topographical features improve the sealing performance. Namely, a turned against a flat surface topography leads to highly localized contact areas, which in turn yields the best sealing performance.

The combination of experimental data with the validated model leads to much deeper insights for the sealing mechanisms than what could be obtained using either on their own.

# 1 Introduction

A (new) casing connection is commonly tested and qualified before it can be used in well construction. Connection testing is often done as per API 5C3 or ISO 13679 [1] standards. The standards define four Connection Assessment Level (CAL)s indicated with an increasing Roman numeral corresponding to increasing severity. CAL I is used to qualify connections for wells for which only moderate internal pressures and axial loads are expected. CAL IV is used to qualify connections for demanding high pressure high temperature applications, which pushes the loading to the connection's structural and sealability limits. Once a qualification is obtained it is only valid for that CAL or lower and for the specific tribosystem tested [2,3], i.e. for a specific material grade, connection type, wall thickness, thread compound and coating. Rules do exist for extrapolation/interpolation to another material grade or wall thickness. Even when using them, however, at least a single specimen test typically needs to be performed to prove the integrity of such new combination [1].

The CAL tests entail the simulation of several well scenarios that are imposed on the full-scale connection by assembly tests in a power tong and by structural and tightness performance tests in a specialized load frame. The casing connection undergoes combined loading, including internal ($p_i$) or external ($p_e$) pressure and tensile ($F_T$) or compressive ($F_C$) axial load, while load, displacement and sealability is monitored. A failure is defined if any of the following occurs: the metal-to-metal seal shows galling in the assembly tests, the connection fails structurally (exceeds yield strength) or the connection leaks at a sustained rate larger than 1.2 ml $\text{min}^{-1}$ [1].

The qualification according to the highest level (CAL IV) comes down to approximately 6 months of testing and an investment in the order of a million US dollar, if successful. Further, as the test is decisive on whether the connection can be used in operations, it will steer connection design. Therefore, it is valuable to have available a method that screens connection sealing performance before the actual qualification tests are done and thereby avoid unnecessary tests and costs. In addition, such a method can assist in the design of metal-to-metal seals and connections having an improved performance. This paper introduces and validates a small-scale test set-up and modelling approach that can do so.

Finite element analysis (FEA) has been applied for screening purposes by calculating, for the metal-to-metal seal, the ratio of the average contact stress to applied pressure [4,5]. However, the success or failure of a metal-to-metal seal is governed by other parameters than only contact stress acting between a perfectly flat and a round surface. Engineering surfaces have a surface topography, often with a certain orientation, which affects their sealing performance [6–8]. Moreover, several features can often be identified at different length scales. The hierarchy of scales that will be used in this paper is shown in Figure 1. In this case, the surface topography can be seen as the sum of out-of-flatness, crowning radius, waviness and roughness. We note that all these components play an important role in the performance of the seal and must be accounted for. This means that the addition of surface topography requires a 3D volumetric computational domain to compute the contact stresses up to scale of the roughness. With FEA, the computational effort would become prohibitive quite quickly, because of the high resolution needed to resolve the contact state at the roughness scale.

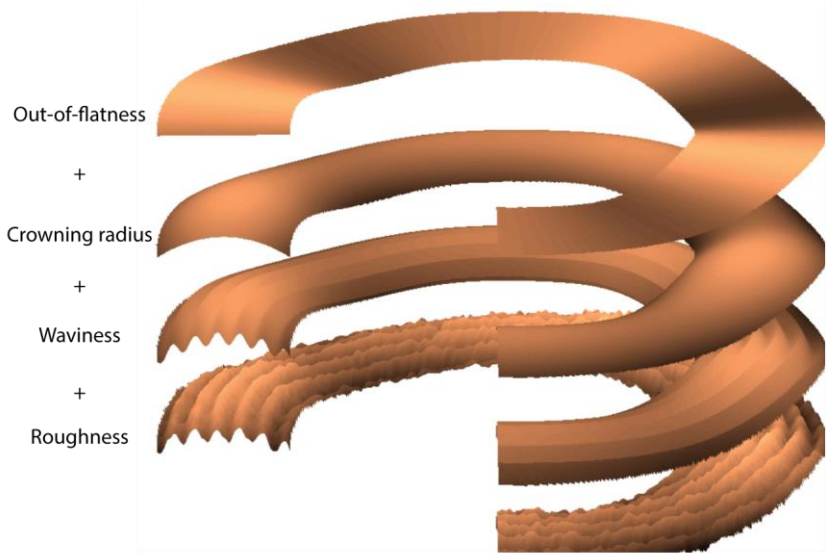


*Figure 1 Hierarchy of scales defining the surface topography in the context of this paper.*

In the modelling approach validated in this paper, the (measured) surface topography is efficiently considered in the contact model using a semi-analytical boundary element method [9], which enables the computation of localized contact stresses and displacements of rough surfaces in contact. The addition of surface topography in the contact simulation allows the introduction of the concept of permeability of the (deformed) gap between the contacting areas of the pin and box of a metal-to-metal seal [10–14]. This permits the definition of a leakage criterion based on permeability instead of a contact stress to pressure ratio, as used in e.g., [4,5]. In addition, it allows the computation of the actual leak rate when combined with the differential pressure and fluid properties [13].

The fundamental work on the sealability model has been presented in previous papers [10–15]. Starting with a deterministic [11] and later a stochastic sealability model [12,15], it was shown that the surface topography and its orientation (e.g. waviness or spiral groove [6], see Figure 1) plays an important role in the sealability of a metal-to-metal seal. The models were used to compare the seal permeability of a surface topography resulting from turning with one resulting from shot blasting. The difference in permeability and thus sealing performance was several orders of magnitude in favor of the turned surface because of the localized contact stresses [12]. In addition, a substantial hysteresis for the sealing performance for loading versus unloading was revealed [14].

The surface topography, and thereby sealability, is affected by the influence of coatings and thread compounds, as these affect the wear process that changes the surface topography during make-up sliding. It was shown, in [16], that optimal sealing can be achieved for the contact combination of a smooth against a wavy surface. The smooth surface is obtained by forming a glaze layer with the phosphate coating on the box [17]. Wear on the bare pin is mild because of the soft coating on the box and the formation of a tribolayer [18], which leaves most of the waviness intact while polishing the tops of such a profile [16]. Next to that, thread compounds improve sealability because of the addition of metallic, metallic oxide or non-metallic inorganic particles [19–22].

To investigate metal-to-metal seals and to validate the sealability model, a test set-up was developed according to the conditions dictated by CAL IV. The conditions were determined using a 9-5/8" casing diameter: a maximum sliding length equivalent to 3 make-ups and break-outs and a final make-up adding up to 1.5 m, sliding velocities in the order of 10 mm $s^{-1}$ using a 2 RPM rotational velocity [23,24] and

contact stresses in the order of 1 GPa at a contact width of 1 – 3 mm [25–27].

The structure of the rest of this paper is as follows. First, the experimental methods and the Shell Sealing Mock-up Rig (SSMUR) test set-up, which were used to validate the model, will be presented. Then, a brief overview of the model will be given. The results obtained with the experimental set-up are discussed next and used to validate the model. Finally, the experimental and model results are combined to discuss the factors affecting sealability of metal-to-metal seals and give new insights on the role of thread compounds in sealability.

# 2 Experimental methodology

In this paper the investigation is aimed at understanding liquid sealability of metal-to-metal seals. The work to obtain this understanding entailed the combination of two parts: small scale experimental sealing tests and the development of a numerical sealing model. In the following, the experimental methodology is presented, which uses a new set-up called the Shell Sealing Mock-up Rig (SSMUR). The numerical methodology can be found in the next section.

## 2.1 Materials and manufacturing of specimens

Specimens were manufactured from thick walled 4" P110 tubing using a lathe. The mechanical properties of the material are given in Table 1. This material was used for all the SSMUR specimens discussed in this paper.

*Table 1 Measured average mechanical properties of the P110 pipe base material according to ISO6892-1* [28].

| Pipe ID | Yield stress Rp0.2 MPa | Ultimate tensile strength Rm MPa | Uniform plastic elongation Ag % | Fracture elongation A5 % | Surface hardness HV10 kg mm$^{-2}$ |
|---|---|---|---|---|---|
| 51876 | 861 | 947 | 6.3 | 18.8 | 306 |

To ensure repeatable surface topography for the test campaign, special attention was given to the metal-to-metal seal surface. This was achieved by specifying the dimensions of the carbide cutting element (tip radius 800 µm), setting a feed rate (120 µm rev$^{-1}$), setting a depth of cut (5 – 10 µm), and using a new cutting element for each specimen.

## 2.2 Phosphating

After manufacturing, some of the specimens were phosphated. For this, the specimens were cleaned, degreased and water rinsed before they were dipped in the zinc or manganese phosphate bath. The process was carried out under controlled laboratory conditions to ensure maximum uniformity and repeatability. The procedure was according to the protocol reported in earlier papers [16–18]. Note that the phosphating modifies the surface topography by removing the waviness. In addition, the roughness is determined by the phosphate crystallites [17].

## 2.3 Lubricants

Thread compound is used in the oil and gas industry to assemble drill pipe or casing connections and is in the basis a grease. In this work, thread compounds and a base oil were used. The lubricants used for assembly of the specimens are listed in Table 2. Because of trade secrets, most commercial thread compounds have undisclosed compositions except for ingredients that need to be stated in the material safety data sheet (MSDS) or that are stated with a general description on the technical data sheet (TDS). A typical grease consists of a base oil, a thickener and additives [29]. In a thread compound the additives are mostly metallic or metallic oxide particles (see Table 2) and are added to improve the assembly

performance and sealability, as discussed in the introduction. The standard thread compound in the oil and gas industry is API modified, which is included as the reference compound. Next to that, a selection of commercially available, environmentally acceptable [30] thread compounds were tested, designated with YD in Table 2. The base oil was used to assess the influence of the thickener and the additives on the sealing performance [31].

*Table 2 Overview of the commercial base oil and thread compounds used in the sealability tests. Data obtained from TDS and MSDS.*

| Short hand | Base oil | Thickener | Additives based on MSDS (particles) | Consistency Cone penetration ($10^{-1}$ mm) |
|---|---|---|---|---|
| O933 | Ondina 933 | - | - | |
| API modified [32] | Mineral oil | Lithium stearate | Lead, copper, zinc, graphite | 310 – 340 |
| YD A | Synthetic polyalphaolefin and ester | Undisclosed | Calcium fluoride, calcium sulphate, calcium carbonate, etc. | 290 – 335 |
| YD D | Undisclosed | Polyurea | Undisclosed | Undisclosed |
| YD E | Undisclosed | Undisclosed | Undisclosed | Undisclosed |
| YD F | Mineral/Synthetic blend | Lithium | Undisclosed | 265 – 300 |

## 2.4 Shell Sealing Mock-Up Rig (SSMUR)

The surface evolution and sealability tests were performed in an in-house developed test set-up called the SSMUR, see Figure 2 for a schematic of the specimens and load frame. Table 3 lists the technical specifications. In this set-up, assembly, micro sliding and sealability can be investigated with scaled (100 mm diameter) metal-to-metal seal specimens at (gas) pressures up to 1500 bar.

*Table 3 Shell sealing mock-up rig technical specifications and limits.*

| Property | Maximum | Resolution (indicated value or better) |
|---|---|---|
| Z-movement (specimen dependent) | - | 0.5 μm |
| Z-force | 120 kN | 750 N |
| Z-torque | 1 kNm | 10 Nm |
| Linear velocity (radius dependent) | 0.1-100mm $s^{-1}$ | - |
| Internal pressure (gas or liquid) | 1500 bar | 1 bar |
| Leak detection | - | 1 mg |
| Specimen diameter | 100 mm | - |

The set-up and experimental design is aimed at mimicking the conditions during an ISO13679 CAL IV test program. The main difference with the CAL tests is that the SSMUR is used to deliberately find the onset of leakage, whereas the CAL is aimed at qualification for leak tightness. The testing can therefore include multiple make-up and break-out cycles to modify the metal-to-metal seal through wear and plastic deformation. In addition, micro-sliding can be imposed to simulate the additional wear caused by the movement as a consequence of (cyclic) mechanical loads. The impact on the sealability can subsequently be quantified by a leakage test using gas or fluid pressure. This is done both to validate the models and to differentiate the performance of different samples. The validated models can subsequently be used to predict sealability of casing connection metal-to-metal seals.

Two configurations are possible: a load-controlled face seal configuration (Figure 2b, Figure 2c) and a position-controlled interference seal configuration (not shown). The interference seal configuration can be a scaled version of a real connection metal-to-metal seal and can be modified to test a wide variety of seal geometries. Both were designed according to the conditions stated in the introduction. The experimental data and model validation presented in this paper are focused on the face seal specimen configuration and will be referred to as the sealability tests for the remainder of the paper. Care has been taken that the actual conditions in a metal-to-metal seal, as discussed above, are well represented in the small-scale test. An overview of the test set-up and testing methodology to achieve these goals is given in the following sections.

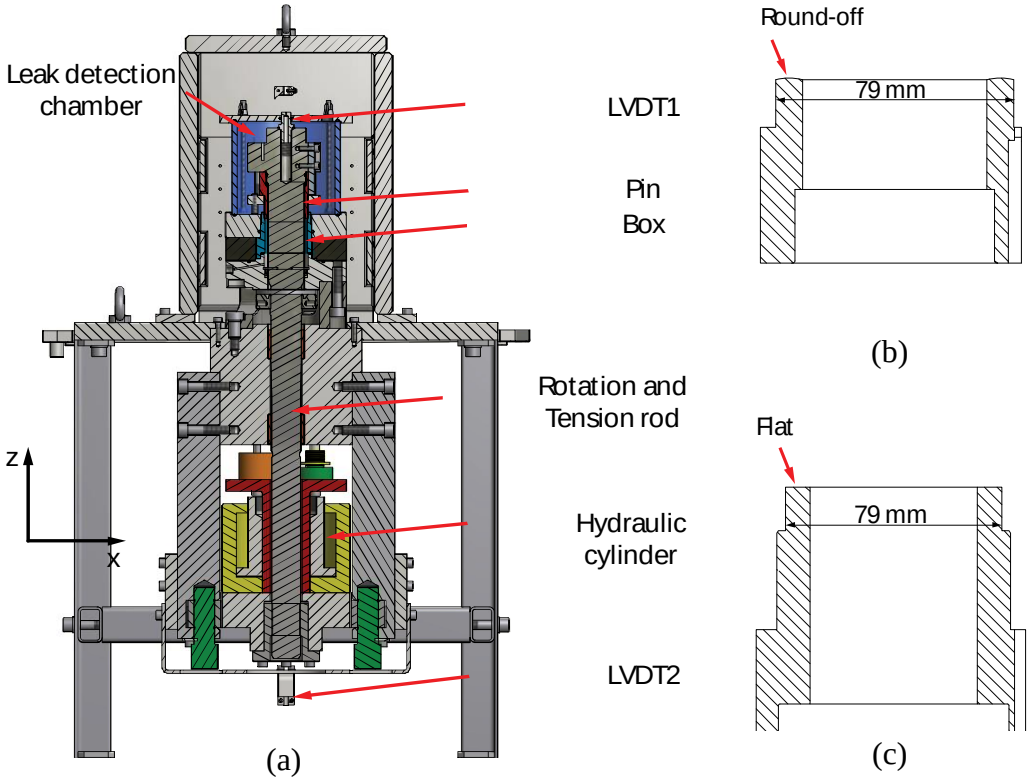


*Figure 2 Overview of the SSMUR load frame and face seal specimens. Figure 2a shows the load frame that is used to execute the experiments with the most important parts indicated. Cross sections on the right show the face seal specimens. Figure 2b shows the top specimen which has a crowning radius associated with a pin. Figure 2c shows the bottom specimen which is flat associated with a box. The circumferential line contact locations are indicated with an arrow.*

## 2.5 Face seal specimens

The face seal set-up or ring-on-ring test [16] provides circumferential line contact at equivalent contact stresses, sliding lengths and sliding velocities as they occur in connection metal-to-metal seals. Assembly is simulated by rotating the top specimen (representing the pin) concentrically on the bottom specimen (representing the box) under a constant load. The conditions are equivalent to the assembly of a casing connector. After "assembly", a sealability test can be performed. The experimental conditions will be described hereafter and are summarized in Table 4.

*Table 4 Summary of face seal experimental conditions.*

| | |
|---|---|
| Geometry | |
| Round-off radius pin | 80 mm |
| Contact line mean diameter | 70 mm |
| Make-up/break-out | |
| Normal load | 30 – 60 kN |
| Contact intensity | 136 – 272 kN $m^{-1}$ |
| Hertzian contact stress (max) | 0.25 - 0.36 GPa |
| Hertzian contact width (max) | 1.4 mm |
| Linear velocity | 24 mm $s^{-1}$ |
| Sealability | |
| Maximum normal load | 120 kN |
| Contact intensity | 546 kN $m^{-1}$ |
| Hertzian contact stress (max) | 0.5 GPa |
| Hertzian contact width (max) | 1.4 mm |
| Temperature | ambient conditions |
| Internal pressure (liquid) | 700 bar |
| Pressurizing medium | Julabo Thermal HS |
| Viscosity | 55 $mm^2$ $s^{-1}$ |
| Density | 0.96 g $cm^{-3}$ |

### 2.5.1 Assembly testing

The line contact configuration is flat against a round-off of R = 80 mm. The contact line diameter is approximately 70 mm and the maximum contact width approximately 1.4 mm. The sliding tests are performed at a contact intensity (CI) of 136 – 273 N $mm^{-1}$ or a maximum Hertzian contact stress of 0.25 – 0.36 GPa by applying 30 – 60 kN normal force. Figure 3 depicts the Hertzian contact stress as function of contact intensity. The sliding velocity was 24 mm $s^{-1}$. The total sliding length is normally 1 revolution or 220 mm unless stated otherwise. It is important to mention that, in contrast with the make-up of a connection, the contact was separated at predefined sliding lengths, to allow taking a replica of the surface topography and monitor the surface evolution. The lubricant was therefore removed and reapplied at each of these steps. Note, however, the focus in this paper is on sealability and that the surface evolution results were presented in an earlier paper [16].

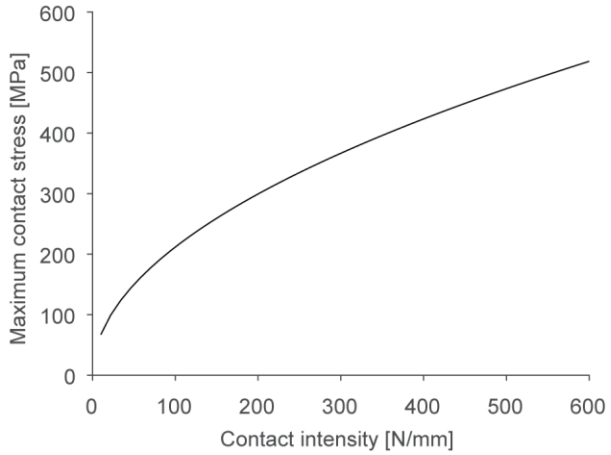


*Figure 3 Maximum contact stress as function of contact intensity for the face seal specimen.*

### 2.5.2 Sealability testing

After assembly, the inside of the specimen was filled with thermal oil (Julabo Thermal HS) and subjected to a 60 – 120 kN normal force corresponding to a 273 – 546 N mm$^{-1}$ contact intensity or a 0.5 GPa maximum Hertzian contact stress. On the outside, the specimen was submerged in a glass leak detection chamber filled with glycol at ambient pressure which acted as leak detection fluid. The glass leak detection chamber was connected with a tube to a beaker on a balance to monitor displacement of the glycol by the thermal oil. An internal fluid pressure of 700 bar was then applied using a pump (Resato BMS). When a steady state was reached, the normal force was gradually lowered in a stepwise manner and the displacement of the glycol was monitored for 15 minutes. The steps were repeated until a leak was observed. The detection of leakage was aided by the density differences of the fluids such that a leak could also be visually detected as shown in Figure 4. The leak location at the onset of leakage was determined using the scale (in degrees) applied around the circumference of the specimen. Droplets (indicated by the arrows) indicate a low leak rate while the foamy streak (encircled) indicates a high leak rate, this was also observed on the balance.

The measurement uncertainties in the contact intensity during the sealability test were determined based on the contributions of the measurement uncertainty in: the load cell, the hydraulic area of the inside of the specimen and the pressure transducer. The result was that measurement uncertainties up 25 N mm$^{-1}$ are possible, which will be indicated with an error bar in the results.

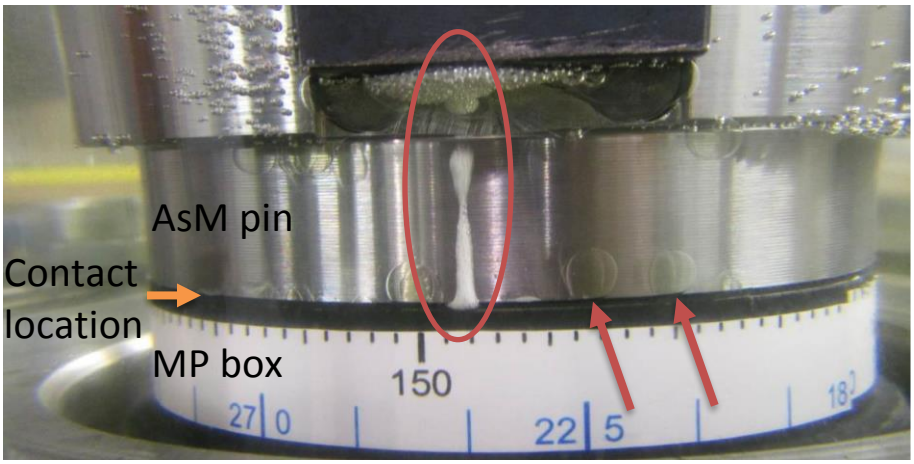


*Figure 4 Example of leak detection with Julabo Thermal HS in Glycol for set FRS05. Pin and box indicated, and the contact location can be observed by the dividing line between pin and box. Two types of leak can be observed. Encircled the foamy high leak rate and, indicated by the arrows, the low leak rate. The leak location was determined using the rotational position in degrees using the applied scale as shown in the picture.*

### 2.5.3 Test matrix

The tests performed are listed in Table 5. Each set of pin and box were given a unique set identifier starting with FRS meaning "Face-seal-Running-in-Sealing" reflecting the specimen type and experimental steps. The pin and box also have a unique five-digit identifier for keeping track of the data. The coating can be Zinc Phosphate (ZP), Manganese Phosphate (MP) or not coated indicated by the As Machined (AsM) tag. The lubricants are following the short hand defined in Table 2. Finally, the data from the assembly phase were summarized by the CI during assembly, the resulting Coefficient of Friction (COF) and the total sliding length. The rationale was to test a wide variety of combinations of coatings and thread compounds to obtain insight in the importance of these parameters on sealability and generate a diverse validation data set for the model.

*Table 5 Overview of the experiments performed with the face seal set-up. Sealability tests were performed with Julabo Thermal HS as pressurizing medium.*

| Set # | Box | Coating[1] | Pin | Coating[1] | Make-up lubricant | $CI_{make-up}$[2] (N/mm) | $COF_{ave}$[3] | Sliding length (mm) |
|---|---|---|---|---|---|---|---|---|
| FRS01[a] | 65297 | MP | 65251 | AsM | O933 | 273 | 0,15 | 1543 |
| FRS05 | 65272 | MP | 65256 | AsM | O933 | 136 | 0,15 | 220 |
| FRS06 | 65273 | MP | 65259 | AsM | API mod | 136 | 0,15 | 220 |
| FRS07 | 65275 | ZP | 65267 | AsM | API mod | 136 | 0,15 | 220 |
| FRS08 | 65276 | MP | 65264 | ZP | API mod | 136 | 0,15 | 220 |
| FRS09 | 65274 | ZP | 65260 | AsM | O933 | 136 | 0,15 | 220 |
| FRS10 | 65289 | AsM | 65266 | ZP | YD-D | 133 | 0,1 | 220 |
| FRS11 | 65284 | MP | 87935 | AsM | O933 | 136 | 0,15 | 220 |
| FRS12 | 65287 | MP | 87936 | AsM | API mod | 136 | 0,15 | 220 |
| FRS13 | 87923 | MP | 87938 | AsM | YD-D | 136 | 0,1 | 220 |
| FRS14 | 87925 | MP | 65252 | AsM | YD-A | 136 | 0,07 | 220 |

[a] Rotated to failure, galling
[1] AsM: As Machined; MP: manganese phosphate; ZP: zinc phosphate
[2] CI: contact intensity
[3] Coefficient of friction

### 2.6 Influence of thread compound on sealability by re-using assembled specimens

For specimen sets FRS11 – FRS14, sealability tests were performed with multiple thread compounds. The first thread compound (listed in Table 2) was used to assemble the specimen and subsequently perform a sealability test. After the sealability test, the contact was opened while keeping the rotational and center position the same. The surface was then cleaned, the next thread compound was applied, the contact was closed again using a contact intensity of 273 N $mm^{-1}$, and another sealability test was performed. This was done 2 – 3 times with each time a different thread compound.

### 2.7 Surface topography before and after the test

To track the changes to the surface topography due to plastic deformation and wear during the test, all specimens were measured before and after the test. The measurements of the surfaces were performed using a Bruker NP-FLEX over an area of 2×3 mm at locations spaced by 120 degrees over the circumference marked by A-B-C. From the area measurements, line profiles were extracted using Matlab. The measurements taken after the test where also used as the topography input for the model.

### 2.8 Contact stress distribution before and after the test

Prior to and after each face seal test the contact stress distribution was determined using FUJiFILM Pressure Measurement Film by applying 10 – 13 kN normal force with the film between the contacting surfaces. This load was chosen to stay within the contact stress range of the film (max 50 MPa). The resulting distribution was analyzed with the accompanying software to obtain the contact stress in MPa from the color intensity of the pressure sensitive chemistry. Based on this result the initial flatness of the contact could be characterized and changes because of wear detected. More importantly, correlations could be made with the location of the onset of leakage.

## 3 Sealing model

A short overview of the sealability model is given here. For details, the interested reader is directed to the previous publications [10–15] as discussed in the introduction. It is important to realize that the sealing model uses the measured surface topography to compute the contact mechanics and subsequently the sealability.

To understand the occurrence of leakage, it must be realized that engineering surfaces are always rough at a microscopic scale, as discussed in the introduction and shown in Figure 5a. Therefore, when the two surfaces are brought into contact, as in Figure 5b, the contact will not be perfect. Instead a certain gap will remain through which the fluid may percolate, Figure 5c. The structure presented in Figure 5 is also the conceptual way in which the model works. The problem is, however, solved in a two-scale manner (see the flow representation in Figure 9). This means that the effect of roughness is accounted for through its permeability, analogous to porous media. For this, the flow through small patches of a rough surface was studied and the result averaged to compute a local permeability. This permeability will, of course, depend on the contact stress applied on the small patch. The larger the contact stress, the smaller the gap and thus the smaller the permeability. Above a certain contact stress, all possible channels are blocked and a seal created.

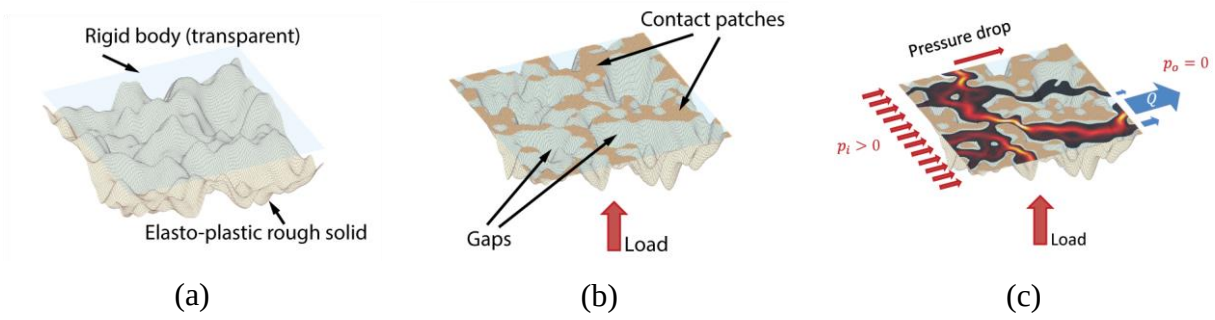


*Figure 5 Overview of the sealing model. (a) Two surfaces are placed facing against each other. Here, a smooth rigid vs. a rough elasto-plastic configuration is used, a rough elasto-plastic vs. rough elasto-plastic configuration is also possible. (b) A load is applied between these two surfaces, leading to contact. This contact is, however, only partial as illustrated by the contact patches. (c) A pressure difference is applied between an inlet ($p_i$) and an outlet ($p_o$). This leads to a certain flow, with a total value Q. Reproduced from* [33].

Once the permeability is known, the surface can be considered smooth, i.e. the information of the roughness scale is now embedded in the permeability. The global contact stress distribution can subsequently be computed at a larger scale, which will be controlled by the geometry of the seal, i.e. its crowning radius and out-of-flatness (Figure 1). Then, the permeability at a certain location can be assessed as a function of the local contact stress or intensity. Once the permeabilities at all locations in the seal are known, the global flow can be computed by making use of the Darcy flow equations and, from it, the total leakage can be obtained. The main differences of the present approach with respect to previous ones is that, although the permeability depends strongly on the contact stress, it also has a random component [12,15].

In the following, a brief explanation is given of the modelling approach used to compute the permeabilities and the total leakage. The problem is separated into two components, i.e. a contact mechanics part to compute the deformed gap left between the surfaces (as in Figure 5b) and a fluid flow through that gap (as in Figure 5c). To separate these two parts, the assumption is that the surface deformations caused by fluid pressure are much smaller than the surface deformations caused by the contact stress.

## 3.1 Contact mechanics

At a given location, the metal-to-metal seal will be subjected to a certain average contact stress. This contact stress can be computed via a FEA or more efficiently, as in the current model, by using a Boundary Element Method (BEM) [34]. The underlying assumptions of the model are that the slopes of the surface topography are small, and that the thickness of the connection is much larger than the typical length of the contact. Both conditions are usually met for engineering surfaces. The material behavior is assumed to be elastic-perfectly plastic. It can thus be modelled through the elastic modulus and the surface hardness [9].

### 3.2 Permeability of the gap

The contact mechanics model thus gives the gap between the two loaded and deformed surfaces. The flow through this gap is subsequently computed to obtain the permeability. To do so it is assumed that the size of the gap is much smaller than the size of the seal, also known as the lubrication approximation. It is further assumed that the gap only contains the pressure medium, meaning the influence of the lubricant is not considered. This leads to the Reynolds equation, which allows the solution of a three-dimensional flow problem while discretizing only the two-dimensional surface [35]. In addition, it is assumed that the pressure medium is a liquid, and that it can be modelled as incompressible. The total flow can then be used to obtain the local permeability. Once the permeability for several of these small rough patches is known, the flow through the whole seal can be computed. This can be expressed by,

$$Q = K\frac{\rho}{\eta}\Delta p, \tag{1}$$

where $Q$ is the total leakage, $K$ is the permeability of the whole seal, based on that of the small patches, $\Delta p$ is the pressure differential over the seal, $\rho$ is the density of the pressure medium and $\eta$ is its viscosity. The main goal of the model is to compute $K$ [11].

### 3.3 Leak rates and treating different pressure media

Compressible media can be handled within this framework by deriving an appropriate scaling which also depends on the absolute pressures at the inlet and outlet as compared to equation ( 1 ). This is especially relevant in the case of nitrogen, which is commonly used as a pressure medium in CAL tests and which cannot be considered incompressible. In [13], it was shown that the total leakage of a fairly general type of fluid can be computed by replacing the pressure difference by a generalized formula that takes into account the compressibility. For the particular case of nitrogen, which can be modelled as an ideal gas, the total leakage was found to be,

$$Q = K\frac{\rho_o}{\eta_o}\frac{p_i^2 - p_o^2}{2p_o},$$

where $p_i$ and $p_o$ are the inlet and outlet pressure and $\rho_o$ and $\eta_o$ are the pressure and viscosity of the fluid at the outlet pressure. The scaling for nitrogen is thus quadratic in $p$ versus linear for incompressible fluids, as shown above. For other fluids, equally simple, although different, expressions can be found, see [13].

The relevance of this formulation is that the conclusions presented in this paper, which concerns only a liquid as a pressure medium, can be readily extended to cases where gas is used as a pressure medium by using the right scaling. This scaling, however, is very large, making it clear that it requires significantly higher contact stress to seal a gas compared to a liquid.

## 4 Results and discussion

The experimental results obtained with the SSMUR set-up will be discussed in the following sections. After that they will be used to validate the sealability model. The combined results are then used to give deeper insight in the sealability mechanisms of metal-to-metal seals.

### 4.1 Correlation of contact stress distribution and leak location

The circumferential contact stress distribution before and after assembly was made visible using FUJiFILM prescale contact stress sensitive film. For each specimen a normal load of 10 – 13 kN was applied to stay below the 50 MPa maximum contact pressure for the pressure sensitive chemistry. A typical result is shown for FRS09 in Figure 6 before and after assembly. The variation in contact stress distribution is the result of the combined out-of-flatness (in the order of microns) in the pin and box

specimens. This resulted in local deviation from the mean contact stress. Here a three-lobe pattern was visible before the test (Figure 6a) that persisted after the assembly tests (Figure 6b). The leak location is indicated with an arrow in Figure 6b. It was found that in almost all the experiments, to be discussed in Section 4.2, the first leakage occurred at a location of lowest or lower contact stress relative to the mean. An exception was FRS12, where the leak occurred at a location of higher contact stress because of localized damage to the surface, which will also be discussed in the next section. The relative differences with the mean contact stress were used to include the influence of out-of-flatness in the model.

The results indicated that reduced out-of-flatness would have improved the sealing performance of all specimens because of a higher mean contact stress. The seal performance is directly related to local contact stress and will be further elaborated with the model results in Section 4.4. In general, it is therefore important to have small form errors in a metal-to-metal seal.

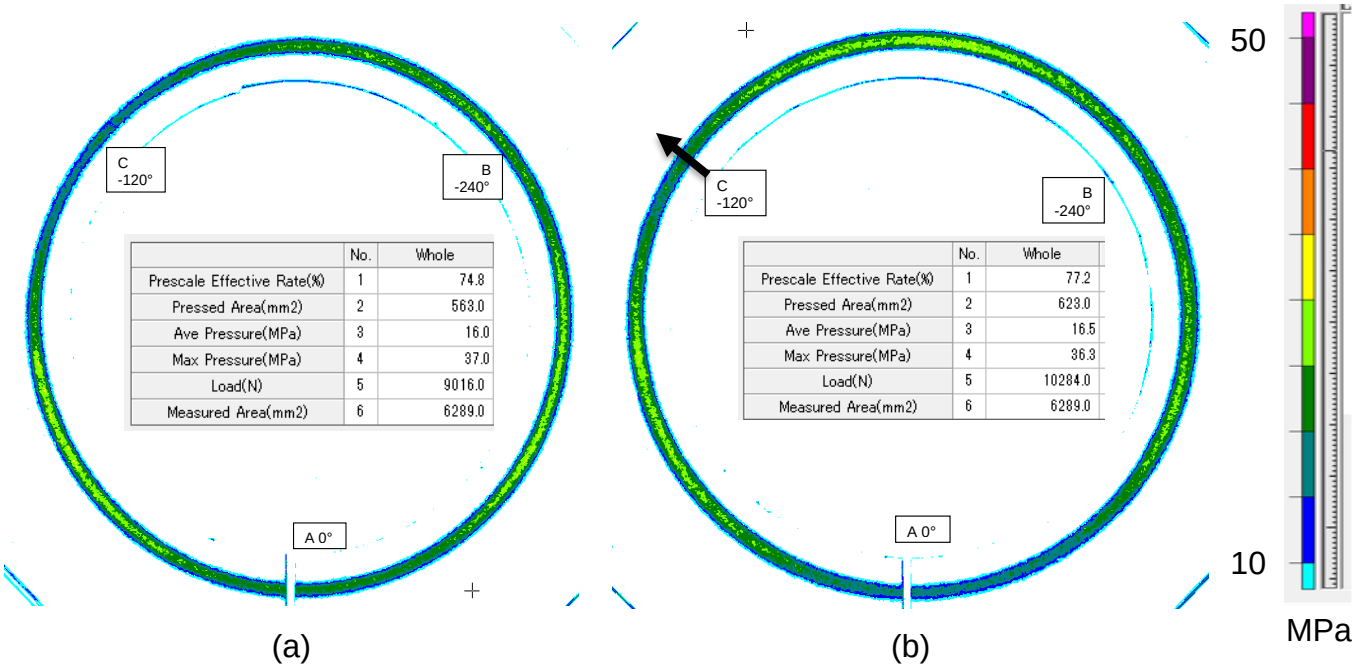


*Figure 6 Overview of contact stress distribution (in MPa) because of out-of-flatness visualized for set FRS09. FUJiFILM Prescale was placed between the pin and the box specimen at a normal load of 10 – 13 kN. (a) Before assembly. (b) After assembly, the arrow indicates the locations of the first observed leaks for each specimen.*

## 4.2 Sealability experiments

The results presented in Figure 7 show the effect of surface topography, thread compound, phosphate coatings, plastic deformation, and wear on the sealability of the metal-to-metal seal system. A leak typically started by first expelling the lubricant after which leakage of the pressure medium followed. This could be observed through the glass leak detection chamber. The sudden removal of the thread compound indicated its blocking capability up to a certain threshold and is consistent with the results by [20,31]. The clean mineral oil O933 does not have this property and was therefore added to the test matrix.

Experiment FRS01 was preceded by an assembly to failure by sliding 1543 mm. A leak test was still performed to obtain a worst-case sealability base line. The subsequent sealability test showed leakage at the highest normal load applied in the test. This was because of the large surface separation or gap created by the surface damage.

The uncoated turned surfaces (FRS06-07 and FRS09-14) only underwent changes locally, at the peaks of the waviness, which generally resulted in a better sealing performance. This can be seen most clearly for

the pins of tests FRS11 – 14 which have identical turned roughness and the local changes are indicated for FRS11. Comparing the 4 tests, we notice that the line profile of test FRS12 (API modified) shows damage to one of the peaks. A large scratch was found at this location which removed the peak. On the box a clear indication of ploughing could be found suggesting a hard particle as the cause of the scratch. Compared to the other specimens in the series FRS11 – 14, the damage resulted in an earlier onset of leakage, and the leak did not occur at a location of lowest contact stress. Comparing FRS09 and FRS11, they differ by the waviness of their turned surface topography. Where FRS09 has less sharp peaks compared to FRS11.

Experiments FRS05, FRS09 and FRS11 all used the same lubricant, i.e., O933. Despite that, the performance of FRS05 is worse compared to both FRS09 and FRS11. The same was observed for FRS08 as compared to FRS06, FRS07 and FRS12, where API modified was used. The reason for this was attributed to the fact that FRS05 and FRS08 did not have a distinct waviness and therefore showed an earlier onset of leakage with the same lubricant, as discussed in [16].

As a general observation, it was found that the sets assembled with API modified performed worse in the sealability tests compared to the environmentally acceptable thread compounds, which is consistent with the results of [19]. This was mostly because of localized surface damage, as discussed above, likely by hard particles in the formulation.

Finally, the results presented above suggested that preserving the waviness is beneficial for sealability. Moreover, the sharper the waviness, the better the sealability of the system. This trend even holds up to the point that even a clean mineral oil shows good sealing performance. This will be further elaborated with the model in Section 4.4 after its validation.

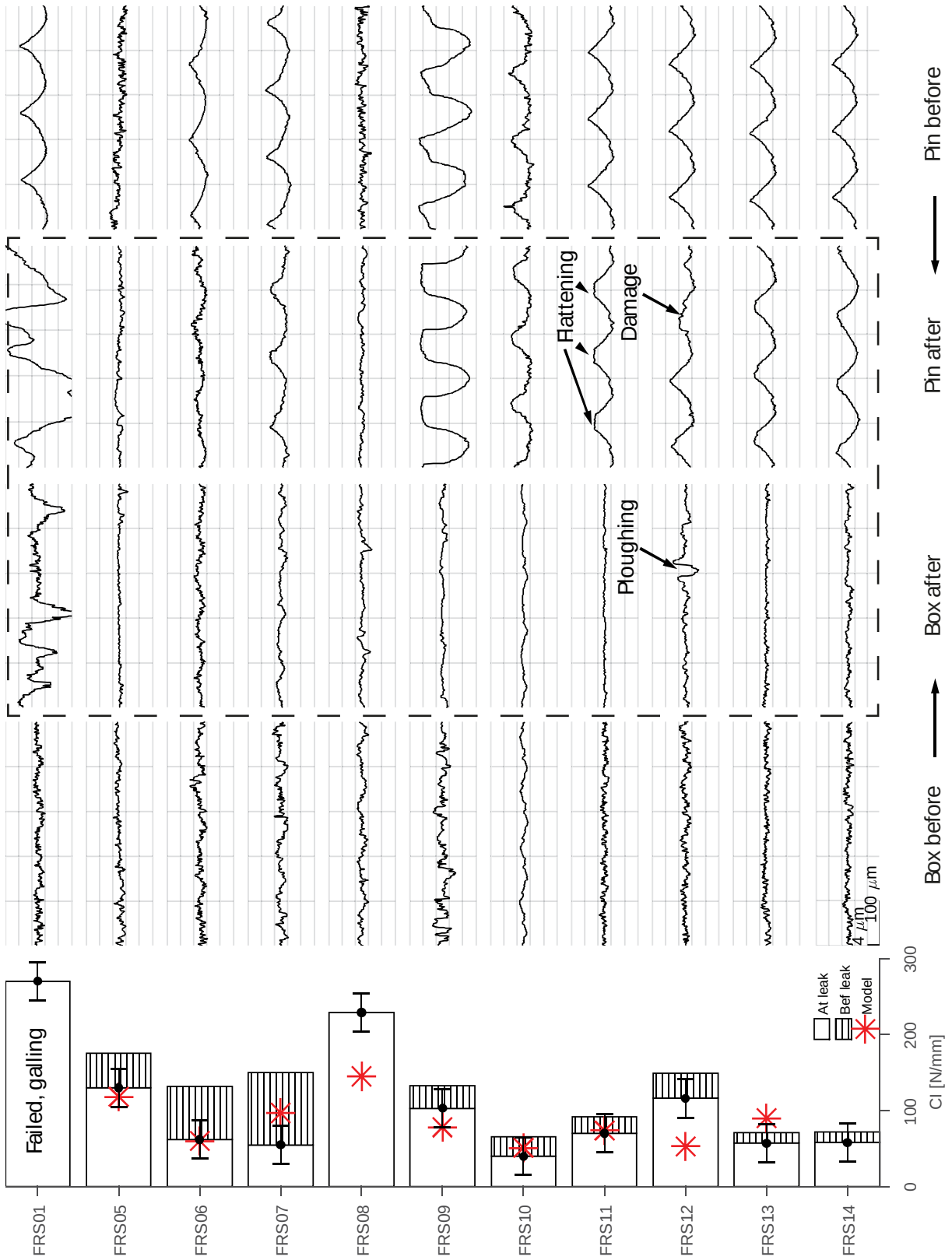


*Figure 7 Overview of the test outcomes, refer to Table 5 for the specimen configuration and assembly lubricant used. Columns represent an experiment as numbered on the bottom. Rows compare the topography before and after the test as indicated at the right. Presented are a bar chart with the contact intensity just before the leak and at leak. The lower the contact intensity at leak the better the performance of the metal-to-metal seal. Connected to the results are shown a cross section of the surface topography of pin and box before and after the test for a matching location on the circumference. A visual correlation can subsequently be made between onset of leakage and surface topography after make-up sliding.*

## 4.3 Overview of influence of thread compounds on sealability

The influence of the thread compound was investigated by reusing the run-in surfaces of the identical sets FRS11 – FRS14 with another thread compound and performing again a sealability test. Note that in these tests the capacity of the thread compound to directly contribute to sealing, instead of their contribution through modified wear conditions, was investigated, as no further make-up was performed. The results are shown in Figure 8. The first bar in the set is the sealability result (using $CI_{at\ leak}$) directly after make-up with the thread compound indicated. The bars next to the first show the results of the subsequent tests with the same surface topography (only closing the contact with a normal load after application of the lubricant) but other thread compounds.

FRS11 showed a relatively good sealing performance in the initial test with O933 (Figure 7). An improvement was found when testing with YD-D. The subsequent results with API-modified indicated reduced sealability performance. The reason for this was that the metallic particles were bearing a substantial part of the normal load. The result was a relatively large gap between the surfaces leading to earlier leakage in the test.

When API-modified is used as the initial thread compound in FRS12, the sealability result improved with respect to FRS11 despite the surface damage (Figure 7) which indicated that API-modified benefits from the make-up phase by smearing out the soft metallic particles. This reduced the fraction of particles bearing the load and thereby the gap between the contacting surfaces. The resulting film can also aid in reducing the roughness of the surface, improving sealability. The performance of this sample was, however, still the worst in the series, because of the damage (scratch) that occurred in the seal. Interestingly, the performance was better when using the clean mineral oil (O933) or the environmentally acceptable thread compound YD-D on the same (damaged) surface. The reason for this is unclear. It can be speculated that, even though API-modified performs better after make-up, the large particles still present a detrimental effect. It could also indicate that YD-D provides better blocking of the scratch, although this would probably imply that cleaning was not complete before applying O933 as no blocking effect was expected by the oil. Possibly, the improvement could also be related to further plastic deformation occurring after the first loading-unloading cycle. However, the effect of plasticity is probably minor after the first cycle. Moreover, this effect should be similar in all four sets in this series and no other set presents this behavior.

The results of FRS13 show a consistent sealability result for all compounds. When repeating the final test with the initial thread compound an improvement in sealability was observed. Set FRS14 indicates that blocking by the thread compound can improve sealing performance to a point where the surface can be taken “out of contact” with a contact intensity at leak of 0 N $mm^{-1}$ for YD-E.

In general, an improvement is observed when a lubricant is applied, and no make-up sliding is performed. Except for API mod and O933. The improvement was attributed to completely filling the gap with thread compound because of only applying normal load. The sliding was thought to reduce the lubricant film in the gap and result in a lower effectiveness in sealing by blocking. FRS13 shows this most clearly where the first and last test were with the same thread compound. For this case, applying thread compound and only normal load improved the sealing performance substantially. In addition, differences in consistency of the compounds in combination with the finite hold time can also affect the sealability outcomes. At the same differential pressure and gap (permeability) a higher consistency thread compound will show low(er) leak rates (as indicated by Equation ( 1 )).

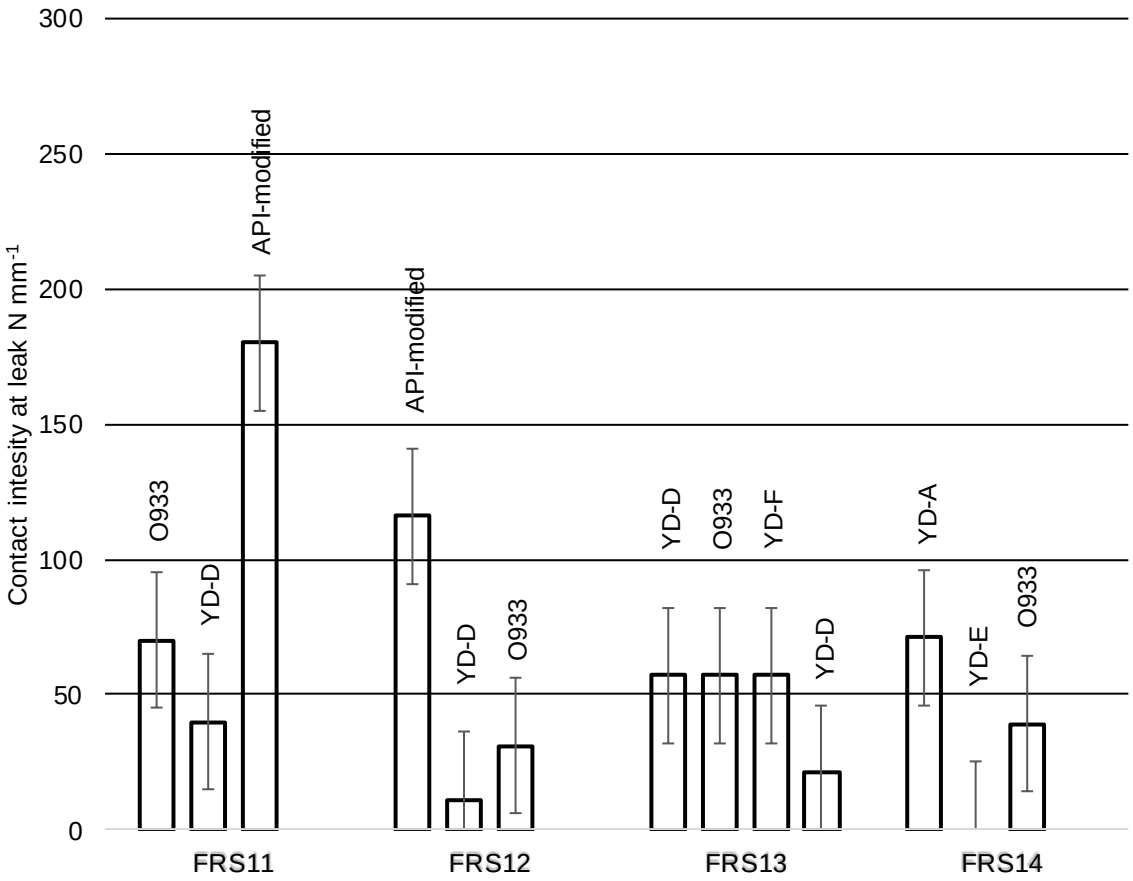


*Figure 8 Results of the thread compound influence tests using the same surface topography with another thread compound. No make-up sliding was performed after the first thread compound, only a sealability test. Tests were performed on the same surface with two additional thread compounds. Only set FRS13 was tested with an additional thread compound. Error bars indicate the measurement error in CI.*

## 4.4 Modelling results and validation

The measured surface topography (Figure 7) was subsequently used as input in the developed model to predict the sealability for each experiment. The leak rate as function of contact intensity was calculated directly for many small patches with the flow model using the applied pressure (700 bar), and the Julabo Thermal HS fluid properties. The leak rate for the whole seal was then computed by summing the results for each patch around the circumference.

The leakage prediction methodology will be discussed by analyzing two representative samples. The corresponding flow patterns are depicted in Figure 9 while the total leakage prediction is shown in Figure 10. Of these samples, one (FRS08) performed poorly while the other (FRS11) only leaked at a small contact intensity.

Before discussing the results in general, first the flow patterns are investigated to understand why one set showed earlier onset of leakage than the other. Focusing first on the flow at very small scales, shown in the inserts of Figure 9, the effect of having clear peaks of the waviness can be seen, even though they are partially flattened because of wear. The set FRS08, in Figure 9a, has a surface topography that does not have clear waviness because of the phosphate coating on both pin and box (Figure 7). Therefore, even if the flow is channelized due to the small size of the gap (see the insert), many channels are available and there is no preferential barrier. In contrast, the set FRS11, Figure 9b, has a clear waviness because of the turned surface topography on the pin and the generation of a glaze layer on the box [16,17] (Figure 7).

This concentrates the contact on the peaks of the waviness and forms a barrier that almost halts the flow (see insert). Only a small channel is available to cross the peak, which makes the overall flow very small. This difference in the local flow has then an impact on the global flow pattern and, therefore, on the total leakage.

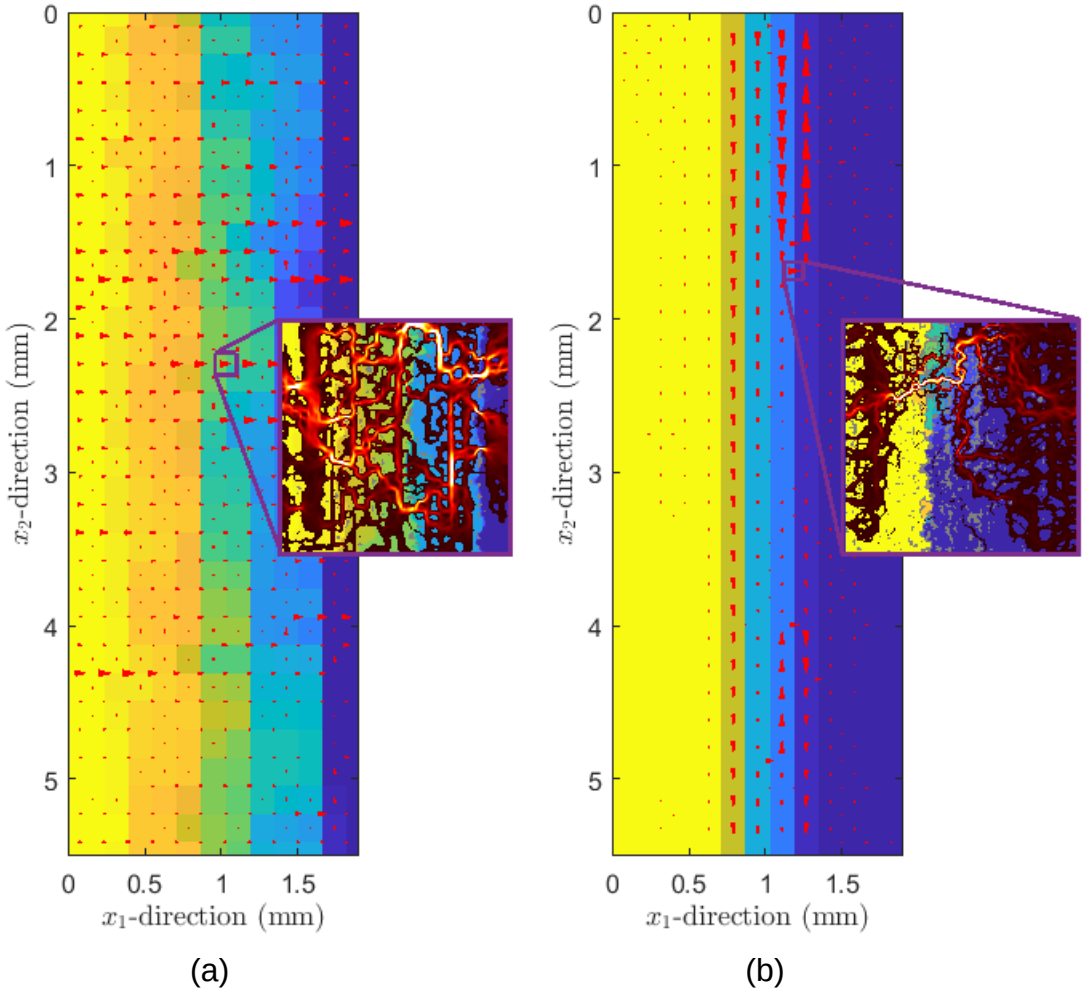


*Figure 9. Representation of the flow pattern as calculated with the model for the sets (a) FRS08 and (b) FRS11. The pressure differential is applied in the radial direction, which would correspond to the axial direction in most connection geometries. Note also that only a fraction of the perimeter in the circumferential direction is shown. The pressure across the seal is depicted in a yellow to blue scale in which yellow indicates the (high) inlet pressure and blue the (low) outlet pressure. The flow rate is indicated by the red arrows, the size of which is proportional to the flow (note that the scaling is different for each set). Since the model is based on a two-scale separation, each arrow summarizes a complex local flow pattern. An example of these is presented in the inlet. There, the yellow to blue scale represents, again, the fluid pressure while the flow is presented in a red scale (again, the scaling is different for each set). The grey spots indicate regions where the surfaces are in contact.*

The global flow for the set FRS08 is mainly radial and the pressure drops constantly from the inlet to the outlet. The flow for the set FRS11 is, however, totally different. The peaks of the waviness form a clear barrier that the fluid cannot always cross. Therefore, it is forced to advance long distances in circumferential direction (even several millimeters) until a channel is found that allows advancing in radial direction. One such event is, for example, marked with a purple square in Figure 9b. This type of flow, which was already observed in [6], forces the fluid to go through a much longer distance and thus leads to a much smaller leakage.

The resulting leak rates versus contact intensity are shown in Figure 10 and will be referred to as J-curves. The leakage corresponding to the set FRS08 (Figure 10a) can be seen to be much larger than that corresponding to FRS11 (Figure 10b). The description of the effect of having the wavy surface topography explains the experimental observations made in Section 4.2. The sets that preserved the waviness exhibited onset of leakage at lower contact intensities. It is important to mention that a lower leak rate is found during unloading because of the accumulated plastic deformation.

Set FRS08 thus exhibits a much larger leakage than set FRS11 at the same contact intensity. The results of the model predictions were subsequently compared with the experimental results in Figure 7. The predicted trend matches with the experimental observations, since the set FRS08 performed much worse in the experiments, as also predicted by the model.

Comparing both sets independently with their experimental result reveals the following. For set FRS08 (Figure 10a), a large leak rate, around 1 ml $min^{-1}$, was computed even at the highest loads. This leakage is detectable by the SSMUR and was indeed observed at maximum load (Figure 7). The model result thus matches the experimental observation. The other case, shown in Figure 10b, is a bit more complex to interpret. The leakage is much smaller but not zero at the highest load.

To reconcile this result with the experimental observation, it is important to realize that there is a thread compound between the two surfaces of the metal-to-metal seal. As shown by Inose et al. [20], Murtagian et al. [31] and discussed in Section 4.3, the thread compound aids with sealing by blocking the gap between the two surfaces. Recall that the flow occurs only through small channels (Figure 9), especially in cases such as the set FRS11, in which the predicted leakage is very small. If these channels are small enough, the thread compound will be able to withstand the pressure and block any leakage through them. Conversely, if they are large enough (as for the set FRS08), it will be pushed outside, and leakage will occur.

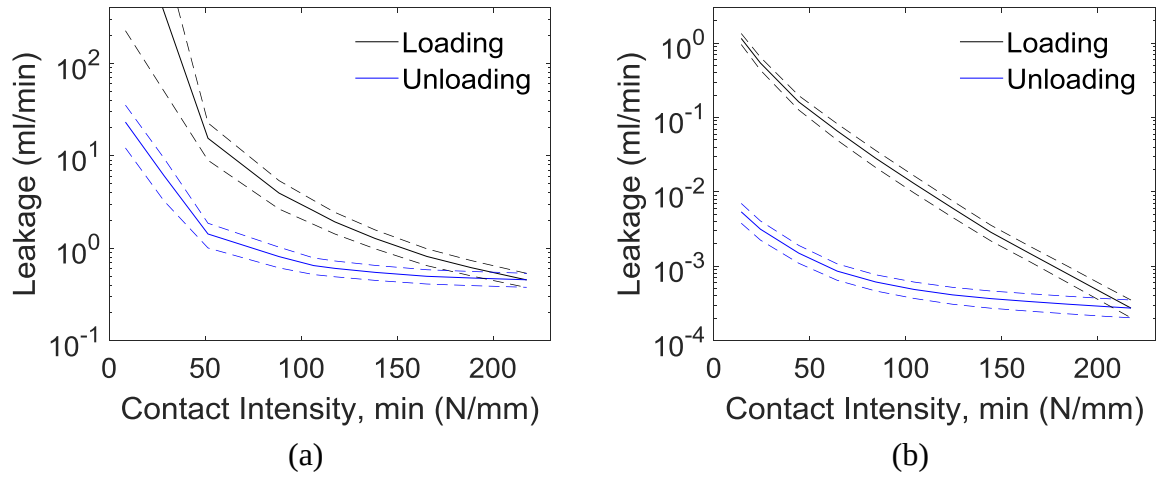


*Figure 10. Leakage versus contact intensity obtained with the model described in Section 3. Shown are the results for (a) FRS08 and (b) FRS11.The loading curve, i.e., the leak rate as the contact intensity increases, is shown in black. The blue curve shows the unloading curve, in which the contact intensity is reduced. The dashed lines indicate the uncertainty in the model prediction, caused by the stochastic treatment of permeability.*

The following hypothesis was formulated based on these observations: there exists a critical channel size, above which the thread compound can no longer block the flow and leakage is observed in the experiment. The permeability (and thus the leakage as presented in Figure 9) is a good indicator for this critical channel size. Therefore, it could also be considered that, above a certain permeability, the thread compound can no longer block the leakage. Large leakages, like the ones computed for the set FRS08, cannot be blocked by the compound. It is only the very small leakages as the one computed for the set FRS11 that are

expected to be blocked.

The unloading curves in Figure 10 give insight in what happens when thread compound is involved and can be used to predict the onset of leakage. The leak rate remains almost constant as the contact intensity reduces. At a certain point, however, it starts increasing much faster. In both cases, this is observed between 100 – 50 N mm$^{-1}$. As shown in [13], this increase in leak rate is characterized by a very rapid increase in the size of the gap. According to the hypothesis, the onset of leakage will occur at some point during this rapid increase. The onset of leakage is thus correlating with the contact intensity at which the sharp increase starts. Since the increase is so rapid (note that a logarithmic scale is used in Figure 9), this is done with little loss of accuracy. This point was found following the system presented in [13].

Applying this analysis to the other specimens, a good correlation was found between the predicted onset of leakage and the observed leakage in the experiments, as presented in Figure 7. In general, the trends were correctly captured for the variety of conditions tested. Only two exceptions can be identified. One is the case of FRS08. In this case the sharp increase occurs as well but starting from an already very high leakage. Indeed, this set already leaked at the highest contact intensity. It was shown, however, that this can be identified by the leakage prediction (see Figure 9). The other set for which the prediction is not very accurate is FRS12. In this case, however, the leakage probably occurred through a scratch, which was not considered in the model. We can therefore confirm the hypothesis posed early in this section and conclude that the model here considered predicts leakage in a manner that is consistent with experimental observations if the seal is not damaged by large scratches (in which case it will probably fail).

# 5 Conclusions

A sealability model based on the concept of permeability of the rough deformed gap resulting from the contact of a metal-to-metal sealing element in a casing connection has been successfully validated using experimental data.

The experimental and model results show that the sealability of metal-to-metal seals is affected by:

1) Surface topography. The waviness of a turned surface gives rise to multiple circumferential spiraling lines of highly localized contact stress. This improves sealability compared to a non-structured surface topography such as the combination of two phosphated surfaces. In addition, by having several parallel line contacts inside the contact, the robustness of the metal-to-metal seal is improved.
2) Thread compound. For the first time the influence of thread compound was determined on the same surface topography. Two functions of the thread compound where identified:
   a) Ensuring low wear during the assembly process and thereby preserving the sharp wavy surface topography. This ensures the highly localized contact stress.
   b) Blocking of channels and thereby increasing the critical gap size needed to allow percolation of the pressure medium. The blocking property was shown to be even more relevant for gases as leakage will be much higher for the same surface topography.
3) Form errors or out-of-flatness. The minimum contact stress on the circumference determines the first onset of leakage. This indicates that out-of-flatness should be at least controlled and, when possible, reduced to improve sealability of a metal-to-metal seal.
4) Loading - unloading hysteresis. The model showed that pre-loading the seal to a higher local contact stress than its operating contact stress can improve the sealability of the metal-to-metal seal.

The outcome of this study can be used for the optimization of the design of metal-to-metal seals which should include a wavy surface topography on the pin against a flat surface topography on the box. Provided that these surface topographies are retained during the service life of the connection.

## References


[1] API. Petroleum and natural gas industries - Procedures for testing casing and tubing connections (ISO 13679:2011) Industries. vol. 2011. Geneva: 2011.

[2] Czichos H, Winer WO. Tribology: A Systems Approach to the Science and Technology of Friction, Lubrication and Wear (Tribology Series, 1). vol. 100. Elsevier; 1978. doi:10.1115/1.3453269.

[3] Salomon G. Application of Systems Thinking to Tribology. A S L E Trans 1974;17:295–9. doi:10.1080/05698197408981469.

[4] Schwind B, Payne M. Development of Leak Resistance in Industry Standard OCTG Connections using Finite Element Analysis and Full Scale Testing. Offshore Technol … 2001.

[5] Hilbert LB, Kalil IA. Evaluation of Premium Threaded Connections Using Finite-Element Analysis and Full-Scale Testing. SPE/IADC Drill. Conf., Society of Petroleum Engineers; 1992. doi:10.2118/23904-MS.

[6] Geoffroy S, Prat M. On the Leak Through a Spiral-Groove Metallic Static Ring Gasket. J Fluids Eng 2004;126:48. doi:10.1115/1.1637627.

[7] Marie C, Lasseux D, Zahouani H, Sainsot P. An integrated Approach to Characterize Liquid Leakage Through Metal Contact Seal. Eur J Mech Environ Eng 2003;48:81–6.

[8] Nakamura T, Funabashi K. Effects of directional properties of roughness and tangential force on pressure flow between contacting surfaces. Lubr Sci 1991;4:13–23. doi:10.1002/ls.3010040103.

[9] Almqvist A, Sahlin F, Larsson R, Glavatskih S. On the dry elasto-plastic contact of nominally flat surfaces. Tribol Int 2007;40:574–9. doi:10.1016/j.triboint.2005.11.008.

[10] Pérez-Ràfols F, Larsson R, van Riet EJ, Almqvist A. On the flow through plastically deformed surfaces under unloading: A spectral approach. Proc Inst Mech Eng Part C J Mech Eng Sci 2018;232:908–18. doi:10.1177/0954406217690180.

[11] Pérez-Ràfols F, Larsson R, Almqvist A. Modelling of leakage on metal-to-metal seals. Tribol Int 2016;94:421–7. doi:10.1016/j.triboint.2015.10.003.

[12] Pérez-Ràfols F, Larsson R, Lundström S, Wall P, Almqvist A. A stochastic two-scale model for pressure-driven flow between rough surfaces. Proc R Soc A Math Phys Eng Sci 2016;472. doi:10.1098/rspa.2016.0069.

[13] Pérez-Ràfols F, Wall P, Almqvist A. On compressible and piezo-viscous flow in thin porous media. Proc R Soc A Math Phys Eng Sci 2018;474. doi:10.1098/rspa.2017.0601.

[14] Pérez-Ràfols F, Larsson R, van Riet EJ, Almqvist A. On the loading and unloading of metal-to-metal seals: A two-scale stochastic approach. Proc Inst Mech Eng Part J J Eng Tribol 2018. doi:10.1177/1350650118755620.

[15] Pérez-Ràfols F, Almqvist A, Pérez-Ràfols F, Almqvist A. An Enhanced Stochastic Two-Scale Model for Metal-to-Metal Seals. Lubricants 2018;6:87. doi:10.3390/lubricants6040087.

[16] Ernens D, van Riet EJ, de Rooij MB, Pasaribu HR, van Haaften WM, Schipper DJ. The Role of Phosphate-Conversion Coatings in the Makeup and Sealing Ability of Casing Connections. SPE Drill Complet 2018. doi:10.2118/184690-PA.

[17] Ernens D, de Rooij MB, Pasaribu HR, van Riet EJ, van Haaften WM, Schipper DJ. Mechanical characterization and single asperity scratch behaviour of dry zinc and manganese phosphate coatings. Tribol Int 2018;118:474–83. doi:10.1016/j.triboint.2017.04.034.

[18] Ernens D, Langedijk G, Smit P, de Rooij MB, Pasaribu HR, Schipper DJ. Characterization of the Adsorption Mechanism of Manganese Phosphate Conversion Coating Derived Tribofilms. Tribol Lett 2018;66:131. doi:10.1007/s11249-018-1082-2.

[19] Hoenig S, Oberndorfer M. Tightness Testing of Environmentally Friendly Thread Compounds. SPE Eur. Annu. Conf. Exhib., vol. 1, Society of Petroleum Engineers; 2006, p. 473–80. doi:10.2118/100220-MS.

[20] Inose K, Sugino M, Goto K. Influence of Grease on High-Pressure Gas Tightness by Metal-to-Metal Seals of Premium Threaded Connections. Tribol Online 2016;11:227–34.

doi:10.2474/trol.11.227.
[21] Bollfrass CA. Sealing Tubular Connections. J Pet Technol 1985;37:955–65. doi:10.2118/14040-PA.
[22] API. WI 2317 : Tech Report on LTC / BTC Performance Properties and Leak Resistance. 2006.
[23] Vallourec Oil and Gas. VAM® book 2017.
[24] Tenaris Hydril. TenarisHydril Running Manual 2017.
[25] Assanelli AP, Dvorkin EN. Finite element models of octg threaded connections. Comput Struct 1993;47:725–34. doi:10.1016/0045-7949(93)90354-G.
[26] Dvorkin EN, Toscano RG. Finite element models in the steel industry Part II: Analyses of tubular products performance. Comput Struct 2003;81:575–94. doi:10.1016/S0045-7949(02)00403-0.
[27] Sugino M, Ugai S, Nakamura K, Yamaguchi S, Hamamoto T. VAM ® 21, an Innovative High-performance Premium Threaded Connection for OCTG. 2015.
[28] ISO 6892-1:2009 Tensile testing — Part 1: Method of test at room temperature. Geneva, Switzerland: International Organization for Standardization; 2009.
[29] Lugt PM. Grease Lubrication in Rolling Bearings. Oxford, UK: John Wiley & Sons Ltd; 2012. doi:10.1002/9781118483961.
[30] OSPAR. Guidelines for Completing the Harmonised Offshore Chemical Notification Format (HOCNF). 2015.
[31] Murtagian GR, Fanelli V, Villasante JA, Johnson DH, Ernst HA. Sealability of Stationary Metal-to-Metal Seals. J Tribol 2004;126:591. doi:10.1115/1.1715103.
[32] API. Recommended Practice on Thread Compounds for Casing, Tubing, and Line Pipe. Washington: 2015.
[33] Pérez-Ràfols F. Two-Scale Stochastic Modelling and Analysis of Leakage Through Metal-To-Metal Seals. Luleå University of Technology, 2018.
[34] Polonsky IA, Keer LM. Fast Methods for Solving Rough Contact Problems: A Comparative Study. J Tribol 2000;122:36. doi:10.1115/1.555326.
[35] Sahlin F, Larsson R, Almqvist A, Lugt PM, Marklund P. A mixed lubrication model incorporating measured surface topography. Part 1: theory of flow factors. Proc Inst Mech Eng Part J J Eng Tribol 2010;224:335–51. doi:10.1243/13506501JET658.